Trans-species microRNA loci in the parasitic plant *Cuscuta campestris* have a U6-like snRNA promoter

Collin Hudzik[1,2], Sean Maguire[3], Shengxi Guan[3], Jeremy Held[2,4], and Michael J. Axtell[1,2]

1. Department of Biology, The Pennsylvania State University, University Park, PA, 16802, USA

2. Huck Institutes of the Life Sciences, The Pennsylvania State University, University Park, PA, 16802, USA

3. New England Biolabs, Inc., 240 County Road, Ipswich, MA 01938, USA

4. Department of Plant Pathology and Environmental Microbiology, The Pennsylvania State University, University Park, PA, 16802, USA

Corresponding Author: Michael J. Axtell, mja18@psu.edu

Short Title: Common promoter for *trans*-species *MIRNA*s

The author responsible for distribution of materials integral to the findings presented in this article in accordance with the policy described in the Instructions for Authors (https://academic.oup.com/plcell/pages/General-Instructions) is: Michael J. Axtell (mja18@psu.edu).

Abstract

Small regulatory RNAs can move between organisms during pathogenic interactions and regulate gene expression in the recipient. If and how such "*trans*-species" small RNAs are distinguished from normal small RNAs is not known. The parasitic plant *Cuscuta campestris* produces a number of microRNAs that specifically accumulate at the interface between parasite and host, several of which have been demonstrated to have *trans*-species activity. We find that induction of *C. campestris* interface-induced microRNAs was similar regardless of host species, and can be replicated in haustoria stimulated to develop in the complete absence of a host. We also find that the loci encoding *C. campestris* interface-induced microRNAs are distinguished by a common 10 base-pair *cis*-regulatory element. This element is identical to a previously described upstream sequence element used by all plant small nuclear RNA loci. The sequence context of this element strongly suggests U6-like transcription by RNA polymerase III. The element promotes accumulation of interface-induced miRNAs in a heterologous system. This common promoter element distinguishes *C. campestris* interface-induced microRNA loci from other plant small RNAs; other plant small RNA loci are transcribed by polymerases II or IV, and lack any common promoter motifs. Our data suggest that *C. campestris* interface-induced miRNAs are produced in a manner distinct from canonical miRNAs. All confirmed *C. campestris* microRNAs with confirmed *trans*-species activity are interface-induced and possess these features. We speculate that this distinct production may allow these miRNAs to be exported to hosts.

Introduction

Small regulatory RNAs are 21 to 24 nucleotide RNAs which play an important role as regulators of gene expression. Plants produce at least three distinct classes of small RNAs. MicroRNAs (miRNAs) are usually 21-22 nucleotides in length and derived from single-stranded stem-loop precursors (Chen, 2005; Axtell, 2013). MiRNAs usually regulate specific target mRNAs post-

transcriptionally. Canonical plant miRNAs are processed from longer primary transcripts. Canonical plant miRNA precursors in *Arabidopsis thaliana* are transcribed by RNA polymerase II, have variable lengths, and besides a TATA box (Xie et al., 2005) lack any common *cis* regulatory elements. There are also two distinct types of short interfering RNAs (siRNAs), both of which originate from double-stranded RNA precursors. Shorter siRNAs are 21-22 nucleotides long, and mostly function outside of the nucleus in post-transcriptional silencing of endogenous mRNAs, aberrant RNAs, and viral RNA (Fei et al., 2013). Longer siRNAs are mostly 24 nucleotides long and usually function in the nucleus to direct *de novo* DNA methylation to transposons and other non-genic sequences (Matzke and Mosher, 2014). *Trans*-species small RNAs, defined as small RNAs that naturally move from one organism to another, play important roles in plant-pathogen interactions by targeting mRNAs in the recipient organism (Huang et al., 2019; Hudzik et al., 2020). Most experimentally verified cases involve miRNAs (Zhang et al., 2016; Shahid et al., 2018) or 21-22 nucleotide siRNAs (Weiberg et al., 2013; Cai et al., 2018; Hou et al., 2019).

Cuscuta campestris is an obligate parasitic plant which uses a specialized organ called the haustorium to pierce the host stem and fuse with the vasculature to feed (Heide-Jørgensen, 2008). The haustorium facilitates bidirectional movement of photosynthates and macromolecules between the host and parasite (Birschwilks et al., 2006; Roney et al., 2007; David-Schwartz et al., 2008; Kim and Westwood, 2015). Haustorium organogenesis is divided into the adhesive, intrusive, and conductive phases (Shimizu and Aoki, 2019). During the adhesive phase, cortical cells from the parasite stem begin to differentiate and divide to form the endophyte primordia. Digitate cells from the endophyte primordia eventually extend through and invade the host stem, marking the transition into the intrusive phase. Digitate cells, now referred to as searching hyphae, continue to extend and move in-between cortical cells to identify the host vasculature (Vaughn, 2003). Searching hyphae will differentiate into xylic or phloic hyphae once in contact with the respective vasculature. Haustoria have fully matured and reached the conductive phase once differentiated hyphae begin to actively receive nutrients from the host (Vaughn, 2006).

C. campestris lacks several miRNA families that are otherwise common in closely related species (Zangishei et al., 2022). Other *C. campestris MIRNA* loci may have been acquired through horizontal gene transfer (Yang et al., 2019; Zangishei et al., 2022). These patterns of loss and gain mirror those observed for *Cuscuta* protein-coding genes (Sun et al., 2018; Vogel et al., 2018). *C. campestris* produces a set of miRNAs specifically at the interface between the host and parasite (Shahid et al., 2018; Johnson et al., 2019), some of which can move long distances in the host plant (Subhankar et al., 2021). Several interface-induced miRNAs from *C. campestris* have been experimentally demonstrated to target and regulate host mRNAs, and thus act in a *trans*-species manner. Host mRNAs involved in biotic defense, hormone signaling, and vascular development are targeted (Shahid et al., 2018; Johnson et al., 2019). A subset of the interface-induced, *trans*-species miRNAs are 22 nucleotides long, which allows for production host-derived secondary siRNAs to accumulate during parasitism (Chen et al., 2010; Cuperus et al., 2010). Analysis of interface-induced, *trans*-species miRNA diversity within and between *Cucuta* species provides clear evidence that several miRNA-target relationships have been under selection (Johnson et al., 2019). When *C. campestris* is grown on a host plants with a non-functional copy of certain targets parasite biomass increases significantly (Shahid et al., 2018). Thus we hypothesize that *C. campestris* uses interface-induced, *trans*-species miRNAs to manipulate host gene expression to increase parasite fitness. We use the term “interface-induced miRNAs” to refer to all such differentially expressed miRNAs because not all of them have been directly proven to target host mRNAs.

In this study we examine the regulation of *C. campestris* interface-induced miRNAs with respect to haustorial development and host identity. We also analyze *cis*-regulatory features found at the loci encoding *C. campestris* interface-induced miRNAs.

Results

Improved annotation of interface-induced *MIRNA* loci from *C. campestris*

A total of 43 *C. campestris* interface-induced *MIRNA* loci, representing 36 distinct families, were previously identified based on a single small RNA-seq experiment with two biological replicates per tissue type (Shahid et al., 2018). Subsequently several more small RNA-seq datasets from *C. campestris* infestation of *A. thaliana* have been produced ((Johnson et al., 2019); Supplemental Table 1). A *C. campestris* draft genome assembly with higher contiguity relative to the one used by (Shahid et al., 2018) has also been described (Vogel et al., 2018). The additional small RNA-seq data were used in conjunction with the improved genome assembly to identify interface-induced *MIRNA* loci. A total of 156 *C. campestris* interface-induced *MIRNA* ("ccm-IIM") loci, representing 103 families, were annotated (Supplemental Datasets 1-3). None of these families have been annotated in other plant species (per miRBase version 22). These improved annotations more than triple the known number of *C. campestris* interface-induced *MIRNA* loci, and include all miRNAs previously shown to target host mRNAs. A total of 21 out of the 103 families have one or more experimental lines of evidence supporting *trans*-species activity against host mRNAs (Shahid et al., 2018; Johnson et al., 2019; Figure 1; Supplemental Table 2). All data are searchable with genome browsers and integrated small RNA visualization tools at https://plantsmallrnagenes.science.psu.edu/Studies/Hudzik.

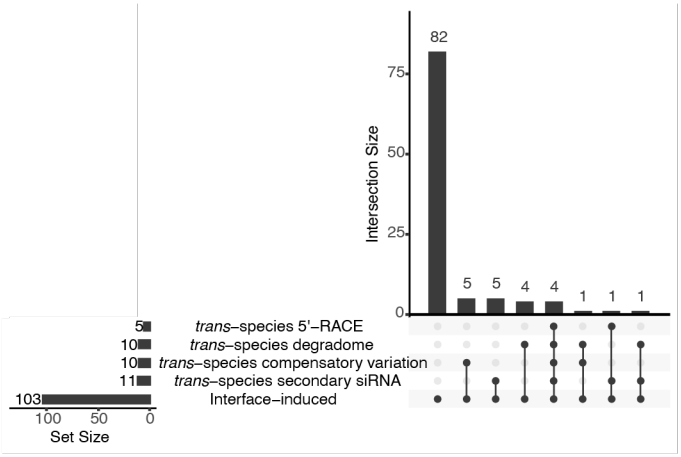

Figure 1: Evidence for *trans*-species targeting of host mRNAs by *Cuscuta campestris* interface-induced miRNA families. See Supplemental Table 2 for details.

C. campestris interface-induced miRNAs accumulate prior to host penetration

Whether using *A. thaliana* inflorescence stems or *Solanum lycopersicum* hypocotyls as a host, haustorium organogenesis progressed at the same rate (Supplemental Figures 1-2). Haustoria were in the adhesive phase during days 0-2 of the time-course when the formation of the endophyte primordia was observed (Figures 2A, 2D). The intrusive phase, discerned by searching hyphae invading the host cortex, spanned days 3-5 (Figures 2B, 2E). A xylem bridge connecting host and parasite vasculature via the haustorium was not detectable until day 6 (Figures 2C, 2F); this marks the start of the conductive phase.

sRNA sequencing was performed across a 15-day time-series (days 0-14) of *C. campestris*-host interfaces for both *A. thaliana* and *S. lycopersicum* hosts. Interface-induced miRNAs began accumulating in the adhesive phase, and reached maximum levels by the start of the intrusive

phase (Figure 2G, 2H). Interface-induced miRNAs can stimulate the generation of secondary siRNAs following an initial cleavage event on a host transcript (Shahid et al., 2018; Johnson et al., 2019). Appearance of secondary siRNAs must therefore occur after miRNAs interact with host mRNAs. Accumulation of secondary siRNAs did not begin until the intrusive phase, and did not reach maximum levels until the conductive phase (Figure 2G, 2H). These data show that interface-induced miRNAs appear early in haustorial development, before any penetration of host tissue has occurred.

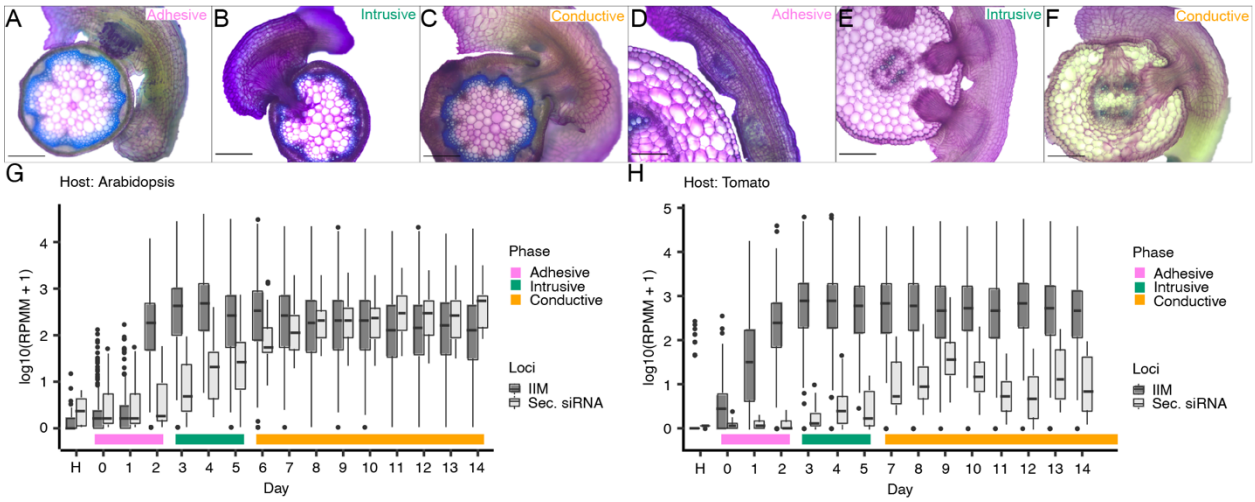

Figure 2: Interface-induced miRNAs are detectable during the adhesive phase. Histological sections of haustoria growing on *A. thaliana* (A-C) and *S. lycopersicum* (D-F). Top right text in each image (A-F) denotes the stage of haustorium organogenesis, the color correlates with the phases labeled in G and H. (Scale bars: 200µm) (G, H) Detection of interface-induced miRNAs (IIM) and secondary siRNAs (Sec. siRNA) using *A. thaliana* or *S. lycopersicum* as hosts. Boxplots show medians (central line), 25th-75th percentiles (box boundaries), up to 1.5x the interquartile range (whiskers), and outliers (dots). RPMM: Reads per million mapped. Histological sections from the full time-course, including the images shown in A-F, are shown in Supplemental Figures 1-2.

C. campestris interface-induced miRNA induction is not host-dependent

C. campestris has a broad host range. One possible method of adapting to diverse hosts could be to adjust interface-induced miRNA accumulation depending on the host species. This hypothesis was tested by plotting the median conductive phase small RNA accumulation levels of each interface-induced *MIRNA* locus from tomato and *A. thaliana* hosts. The resulting plot showed a linear correlation (Figure 3A), where each *MIRNA* locus accumulated miRNAs to similar levels with either species as a host. This argues against the hypothesis that miRNA induction varies depending on the host species.

Detached shoot tips of *C. campestris* can be stimulated to differentiate haustoria by specific light and tactile stimuli (Figure 3B; (Kaga et al., 2020)). These *in vitro* haustoria can be produced either with or without adjacent host tissue, such as detached host leaves (Figure 3B). *In vitro* haustoria produced with or without adjacent *A. thaliana* leaves were processed in triplicate for small RNA sequencing to test interface-induced miRNA accumulation. *C. campestris* shoot tips (also in triplicate) were used as a negative control. Interface-induced miRNAs were abundant in *in vitro* haustoria regardless of the presence or absence of detached host leaves (Figure 3C). Median accumulation levels of individual miRNAs were highly correlated between *in vitro* haustoria produced with or without adjacent host tissue (Figure 3D). These observations demonstrate that *C. campestris* interface-induced miRNA production is independent of any host. Instead, their sudden appearance during early haustorial development is part of an inherent developmental program.

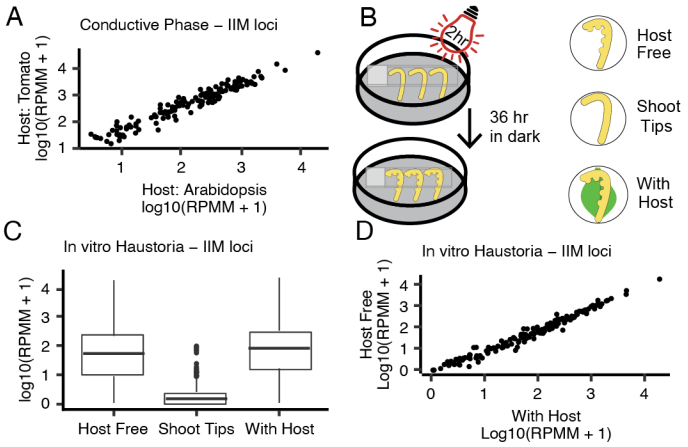

Figure 3: Interface-induced miRNA production is independent of a host. (A) Comparing interface-induced miRNA population and abundance between hosts. Each dot represents the median value of conductive phase samples for an interface-induced miRNA from the sRNA-seq time-course. (B) Graphical overview of *in vitro* haustoria experiment. (C) Interface-induced miRNA accumulation from *in vitro* haustoria. Boxplots show medians (central line), 25th-75th percentiles (box boundaries), up to 1.5x the interquartile range (whiskers), and outliers (dots). (D) Comparing interface-induced accumulation between the Host Free and With Host *in vitro* haustoria. Each dot represents the median value across all replicates for a single interface-induced microRNA from sRNA-seq of *in vitro* haustoria. IIM: Interface-induced microRNA; RPMM: Reads per million mapped.

C. campestris interface-induced *MIRNA* loci share a common upstream sequence element known to control snRNA transcription in plants

Genomic DNA sequences upstream of the interface-induced loci were analyzed with MEME (Bailey et al., 2009) to search for over-represented sequence motifs. Transcription start sites for these *MIRNA* primary transcripts were initially unknown, so the ends of the upstream regions were defined by the 5' basal DCL cut site on the *MIRNA* hairpins (Figure 4A). A highly overrepresented ten nucleotide motif was discovered (Figure 4B). This motif, termed the Upstream Sequence Element (USE), was found adjacent to most (145/156) of the interface-induced *MIRNA* loci (Figure 4C). As a control, a set of 37 "canonical" *MIRNA* loci from *C. campestris* were annotated (Supplemental Dataset 4). These canonical loci encode miRNAs universal among dicots such as miR156, miR164, and miR166. None of the canonical *MIRNA* loci had the USE in their upstream regions (Figure 4C). The motif has a strong tendency to be located ~100 base pairs upstream of the 5' basal DCL cut sites of the interface-induced *MIRNA*s (Figure 4D). A previous study produced nanoPARE data from *C. campestris* / *A. thaliana* haustorial interfaces (Johnson et al., 2019); nanoPARE is an RNA-seq method that captures 5' ends of RNAs. These data were analyzed to find the 5' ends of *MIRNA* primary transcripts. There was a clear peak of nanoPARE data around 40 base-pairs upstream of the 5' basal DCL cut site of the interface-induced *MIRNA*s (Figure 4E). No such peak was apparent when analyzing the canonical *MIRNA* loci (Figure 4E). This analysis suggests that the transcriptional start sites of interface-induced *MIRNA* primary transcripts about 40 bps upstream of the 5'-basal DCL cut site, and thus lie downstream of the USE.

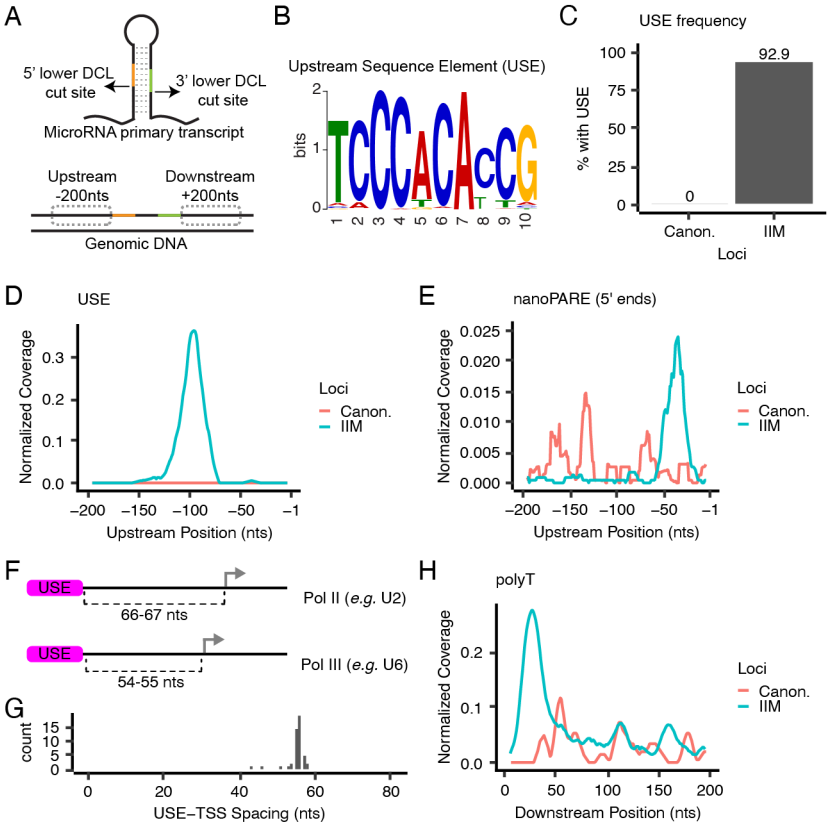

Figure 4: Interface-induced *MIRNA* loci share a *cis*-regulatory element with snRNAs. (A) Schematic showing a *MIRNA* primary transcript (top), and the corresponding genomic locus (bottom). Upstream and downstream regions were anchored by the lower Dicer-Like (DCL) cut sites of the primary transcript. (B) MEME sequence logo of the USE found upstream of interface-induced *MIRNA* loci. (C) Presence of the USE at interface-induced *MIRNA* loci and canonical *MIRNA* loci in *C. campestris*. (D) Metaplot of USE coverage as a function of upstream position. (E) Metaplot of normalized nanoPARE 5' end coverage. (F) Distances between USE and transcriptional start sites (arrows) for known USE-dependent Pol II and III type promoters. (G) Frequency distribution of USE-TSS distances for interface-induced miRNAs. (H) Metaplot of polyT coverage (defined as six or more consecutive T residues on the coding strand) in downstream regions. Canon.: Canonical microRNA loci; IIM: Interface-induced microRNA loci; TSS: Transcriptional start site.

C. campestris interface-induced *MIRNA* loci have features consistent with RNA Polymerase III transcription

The USE found at *C. campestris* interface-induced *MIRNA* loci is identical to a motif known to drive U-snRNA transcription in plants (Vankan and Filipowicz, 1989). U-snRNAs are short non-coding RNAs that, along with associated proteins, form the spliceosome. The spliceosome functions to catalyze intron removal from Pol II-transcribed RNAs during nuclear RNA maturation. The USE is a unique *cis*-regulatory element because it can drive either Pol II or Pol III transcription of U-snRNAs (Waibel and Filipowicz, 1990b). When the USE is 66-67 base-pairs upstream from the transcriptional start site (TSS) it drives Pol II transcription (Figure 4F). When the USE is 54-55 base-pairs upstream of the TSS (one helical turn of DNA shorter), it instead drives Pol III transcription (Figure 4F). *A. thaliana* U2, U4, and U5 snRNA genes contain the longer spacing and are transcribed by Pol II, while *A. thaliana* U6 snRNA genes have the shorter spacing and are transcribed by Pol III (Waibel and Filipowicz, 1990b; Waibel and Filipowicz, 1990a). The TSSs of 48 of the *C. campestris* interface-induced MIRNA primary transcripts were inferred from nanoPARE data (Figure 4E); the rest could not be inferred due to low/no coverage in the nanoPARE data. The USE-TSS distance at these loci had a sharp peak at about 55 base-pairs (Figure 4G), exactly the spacing expected for USE-dependent Pol III

transcription. Pol III termination is triggered by runs of T residues on the non-template strand; four Ts is a minimal signal for termination, and six or more Ts are maximally effective (Gao et al., 2018). Runs of six or more T's were common immediately downstream of interface-induced *MIRNA* loci (Figure 4H). The upstream similarity to U6 snRNA promoters and the prevalence of downstream poly-T stretches suggests that *C. campestris* interface-induced *MIRNA* loci could be transcribed by Pol III.

Accumulation of interface-induced microRNAs in a heterologous system depends on the USE

Agrobacterium tumefacians T-DNA vectors containing *C. campestris* interface-induced *MIRNA* loci were constructed (Figure 5A). The selected miRNAs have both been previously shown to have *trans*-species silencing activity on host mRNAs: miR12463 targets *BIK1* and miR12497 targets *TIR1* and related *AFB* mRNAs (Supplemental Table 2; Shahid et al., 2018, Johnson et al. 2019). The T-DNA did not contain any selectable markers to avoid recruitment of RNA polymerases; transcription of these loci depends solely on any *cis* elements present in the *MIRNA* loci. For each *MIRNA* tested a wild-type and USE-scrambled version were prepared. These T-DNA were introduced to *Nicotiana benthamiana* leaf mesophyll cells by Agro-infiltration. Mature miRNA levels were quantified by qRT-PCR. Mature miRNAs accumulated when wild-type loci were introduced (Figures 5B-C). When the USE element was scrambled, mature miRNA accumulation was dramatically lower (Figures 5B-C). This supports the hypothesis that the USE is a *cis*-acting factor that promotes miRNA accumulation. This result also demonstrates the *C. campestris* interface-induced *MIRNA* precursors can be correctly processed by the RNAi machinery of a heterologous host.

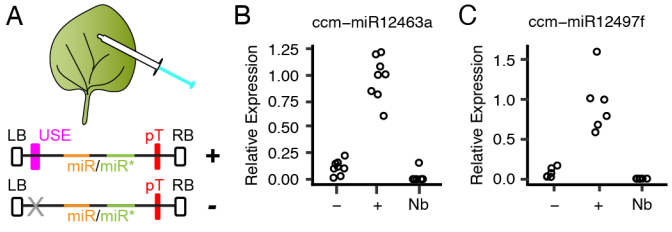

Figure 5: The USE is required for accumulation of interface-induced miRNAs during transient expression in *N. benthamiana*. (A) Graphical representation of constructs used during transient expression. LB: left border; USE: upstream sequence element; pT: polyT stretch; RB: right border. (B-C) Relative expression of miR12463a or miR12497f with scrambled USE sequence (-), wild-type USE sequence (+), and *N. benthamiana* leaf not infiltrated (Nb). Expression was normalized to miR159. Each dot represents a biological replicate (RNAs from a distinct infiltrated leaf).

Discussion

We observed that *C. campestris* interface-induced miRNAs begin accumulating in the adhesive phase, even before the parasite has penetrated the host stem. This suggests that interface-induced miRNAs are primed for immediate use by developing haustoria. Accumulation of interface-induced miRNAs is fully independent of the host identity and does not even require any host. This indicates that their accumulation is a programmed aspect of haustorial development. *C. campestris* is a generalist parasite that feeds on a wide range of host plants. This "shotgun" strategy of miRNA accumulation could be well-suited for a generalist that feeds on diverse hosts. This host-insensitive, shotgun strategy is also consistent with earlier observations of *Cuscuta* miRNA polymorphisms that compensate for most possible variations of target sites within host mRNAs (Johnson et al., 2019).

284 We also found a snRNA-like USE adjacent to nearly all interface-induced *MIRNA* loci. The USE
285 is not found at any canonical miRNA loci in *C. campestris* and has not been reported at *MIRNA*
286 loci in any other plant. The distance between the USE and transcriptional start sites of interface-
287 induced miRNAs is consistent with U6-like Pol III transcription, as is the presence of potential
288 Pol III terminators immediately downstream of most loci. The USE drives accumulation of
289 miRNAs in a heterologous system, directly demonstrating its function as an activating *cis*-
290 regulatory element. We hypothesize that the *C. campestris* interface-induced miRNA precursors
291 are transcribed by RNA Pol III in a USE-dependent manner. All confirmed *trans*-species
292 miRNAs from *C. campestris* are also interface-induced and contain the USE. Only 20% of the
293 interface-induced miRNA families have thus far been proven to target host mRNAs (Figure 1).
294 However, many other targeting events may be undetected. Detection relies on stable sliced
295 remnants of host mRNAs, or on appearance of secondary siRNAs. Some miRNA-target
296 interactions do not cause either outcome. Given their coordinated expression and common *cis*-
297 regulatory motifs, we suspect that many more of the interface-induced miRNAs do in fact target
298 host mRNAs during *C. campestris* parasitism.
299
300 We speculate that the use of Pol III, instead of Pol II, may somehow mark *trans*-species
301 miRNAs for specialized processing and eventual export from the parasite into the host. The
302 *trans*-species miRNAs avoid "self-targeting" of *C. campestris* mRNAs (Shahid et al., 2018;
303 Johnson et al., 2019); this is consistent with the hypothesis that they are made for "export only"
304 and not assembled onto *C. campestris* AGO proteins. The accumulation of mature miRNAs in *in*
305 *vitro* haustoria with no host tissue present directly demonstrates that dicing of the *trans*-species
306 miRNA precursors occurs within *C. campestris*. Therefore, the exported molecule is either
307 mature miRNA or the miRNA/miRNA* duplex.
308
309 Plant U6 promoters are workhorses for constitutive expression of short non-coding RNAs. For
310 instance, the U6-26 promoter from *A. thaliana* is widely used to drive Pol III-dependent sgRNA
311 expression in CRISPR experiments (Tsutsui and Higashiyama, 2017; Lowder et al., 2018). U6-
312 26 has the same USE as the *C. campestris* interface-induced miRNAs (Waibel and Filipowicz,
313 1990a). Indeed, the U6 snRNA is often used as a loading control for miRNA blots, including in
314 the first report of interface-induced miRNAs (Shahid et al., 2018). How does the USE, which in
315 all previously known contexts drives constitutive transcription, result in miRNAs with such a
316 tissue-specific accumulation pattern? One hypothesis is constitutive transcription but tissue-
317 specific dicing of the precursors. However, RNA blots and RNA-seq experiments have yet to
318 detect any strong precursor accumulation in non-haustorial tissues. Resolving the mystery of
319 highly specific accumulation from a promoter that is expected to be constitutive will be an
320 important goal for future research.
321
322 In summary, we find that the *C. campestris* interface-induced *MIRNA* loci are distinguished from
323 canonical *MIRNA* loci by a distinct set of genomic sequence features. This implies that these
324 miRNAs are fundamentally distinct from normal miRNAs and siRNAs. The common promoter
325 element suggests a possible avenue for disruption of *trans*-species miRNA activity: targeting the
326 factors that bind to the USE should reduce production of *trans*-species miRNAs.
327
328 **Methods**
329 **Annotation of *Cuscuta campestris* interface-induced *MIRNA* loci**
330 Annotation of *MIRNA* loci occurred in two steps (early and late) based on the availability of small
331 RNA-seq data during the course of the study. In the early step, previously published small RNA-
332 seq datasets from the interface or parasite stem of *C. campestris* attached to *A. thaliana* were
333 obtained as fastq files from the Sequence Read Archive (SRA; Supplemental Table 1). Trailing
334 3'-sequencing adapters were discovered and trimmed using gsat

335 (https://github.com/MikeAxtell/gsat). Trimmed small RNA datasets were then aligned to the *A.*
336 *thaliana* genome (version TAIR10, including plastid and mitochondrial genomes) using bowtie
337 (Langmead et al., 2009) demanding exact matches and directing unmapped reads to a new
338 fastq file (non-default settings '-v 0 --un'). Small RNA reads that aligned were discarded; this
339 eliminated most small RNAs that could have been produced by the host genome. The remaining
340 reads were analyzed together in a single ShortStack run (version 3.8.5; default settings)
341 (Johnson et al., 2016) using the *C. campestris* genome assembly version 0.32 (Vogel et al.,
342 2018) as the reference genome. This resulted in *de novo* annotation of thousands of discrete
343 small RNA-producing loci. Read counts of aligned small RNAs from each locus in each library
344 were retrieved (from the 'Counts.txt' file produced by ShortStack) and used as input for
345 differential expression analysis using DESeq2 (Love et al., 2014). Differential expression
346 analysis of interface vs. parasite stem was independently performed for each of the three
347 studies included in the first step (Shahid et al. expt.1, Shahid et al. expt. 2, and Johnson et al.;
348 Supplemental Table 1). DESeq2 analysis used 'lfcShrink' using the 'normal' shrinkage estimator;
349 loci up-regulated in interface relative to parasite stem with an FDR-adjusted p-value of < 0.05
350 were called differentially expressed. The union of all three sets of differentially expressed loci
351 from each study was then computed and retained. From these, loci where a) greater than 80%
352 of aligned reads were between 20-24 nucleotides in length and b) the single most abundant
353 aligned RNA size was 20, 21, 22, or 23 nucleotides long were retained. The retained loci were
354 then individually examined using multiple visualization tools: Integrative Genomics Viewer
355 (Robinson et al., 2011), strucVis (https://github.com/MikeAxtell/strucVis), and sRNA_Viewer
356 (https://github.com/MikeAxtell/sRNA_Viewer). Based on the manual examinations, loci that did
357 not conform to all of the guidelines for confident plant *MIRNA* locus annotation (Axtell and
358 Meyers, 2018) were discarded. The late phase of *MIRNA* annotation took advantage of the
359 much greater amount of sRNA-seq data generated during the time-course analyses of *C.*
360 *campestris* on both *A. thaliana* and *S. lycopersicum* hosts (Supplemental Table 1). The same
361 analysis approach was used to identify interface-induced *MIRNA* loci using days 9 and 10 as
362 'Interface' samples and day 0 and "host only" as negative control samples. Loci identified in the
363 late phase were then merged with those obtained in the early phase. All together 156 *C.*
364 *campestris* interface-induced *MIRNA* loci were found (Supplemental Datasets 1-3). These loci
365 and the supporting data can be interactively browsed at
366 https://plantsmallrnagenes.science.psu.edu/Studies/Hudzik.
367
368 The mature 5p-miRNA and 3p-miRNA from each locus was queried against miRBase (version
369 22) mature miRNAs using the SSEARCH function (hosted on the miRBase website), restricting
370 hits to Viridiplantae. The mature 5p-miRNA and 3p-miRNA from each loci were also queried
371 against the "superfamilies" described by (Johnson et al., 2019) using ggsearch36 (from the
372 FASTA package), restricting the search to forward strand hits only; alignments were kept that
373 had less than 3 mismatches. In order to group the loci into families, The mature 5p-miRNA and
374 3p-miRNA from each loci were queried against each other in an all vs. all search using
375 ggsearch36, restricting the search to forward strand hits only. Families were defined by no more
376 than 7 mismatches between a given 5p-miRNA and 3p-miRNA. Based on this analysis the 156
377 loci were grouped into 103 distinct families[1].
378
379 **Plant growth conditions**

[1] *N.b.* for reviewers and preprint readers: Not all of these annotations are homologs of already described miRBase families, so many don't yet have miRBase-registered numbers. These cases are temporarily named "ccm-IIM", for *Cuscuta campestris* interface-induced *MIRNA*s. Upon acceptance, these will be registered at miRBase, and the final miRBase numbers will be substituted into the datasets during final revisions.

380 Host plants grown for time-course experiments, *A. thaliana* (Col-0) and *S. lycopersicum* (IL-8-1-
381 1), were grown at 20-22°C and subjected to 16h photoperiods under cool-white fluorescent tube
382 lighting. *C. campestris* seeds were scarified with sulfuric acid for 1 hour, followed by 5-6
383 washes with water. Scarified seeds were placed in glass petri dishes with moist paper towels
384 and placed in a growth chamber at 28°C with 16h photoperiods under fluorescent tube lighting
385 for 3 days. Emerged seedlings were then transplanted to the base of host plants and
386 supplemented with far-red LED lighting throughout the time-course to allow for attachment.
387
388 **Time-course of *C. campestris* haustoria development**
389 Host plants were grown as described above until inflorescence stems of *A. thaliana* hypocotyls
390 of *S. lycopersicum* were able to serve as hosts for *C. campestris. C. campestris* seedlings were
391 scarified and germinated as described above and were placed at the base of inflorescence
392 stems and hypocotyls under a combination of cool-white fluorescent tube lighting and far-red
393 LED lights. Day 0 of the time-course was defined as the day that *C. campestris* had
394 successfully wrapped around a host. Samples were subsequently collected every twenty-four
395 hours. Each day in the time course included three biological replicates consisting of four
396 interfaces. Samples which were used to create sRNA sequencing libraries were flash frozen in
397 liquid nitrogen and stored at -80°C until total RNA extraction was performed using a BioSpec
398 Mini-Beadbeater and Tri-Reagent (Sigma) following the manufacturer's protocol.
399
400 Samples which were subjected to vibratome sectioning were collected and sectioned within the
401 same day. A .stl file created by (Atkinson and Wells, 2017) containing instructions for 3D
402 printing a mold to embed samples in agarose for vibratome sectioning was printed. Interfaces
403 were placed in the mold and embedded in freshly prepared 5% agarose. Once solidified,
404 excess tissue and agarose were trimmed, and the samples were mounted on a metal block
405 using superglue. Mounted samples were secured with a vice grip in the Vibratome 1000 Plus
406 Sectioning System bath. Samples were submerged in ice-cold nanopure water and sectioned
407 with a thickness of 200µm using Personna 3-Facet Double Edge AccuTec Blades at a blade
408 angle of 15°. Sections were stained with freshly prepared 0.002% toluidine blue on a shaker for
409 ten minutes in 3x4 cell culture plates and rinsed 3-4 times with nanopure water. Sections were
410 observed on a Zeiss AXIO Scope A1 trinocular optical microscope using the 10x objective and
411 imaged with a Jenoptik ProgRes C14 Plus microscope CCD. Image processing to remove
412 excess stained agarose from the background was identical for all images. Scale bar of 200µm
413 was added to all images using ImageJ.
414
415 ***In vitro* haustoria**
416 Stimulation of haustorial development in the absence of host tissues was similar to previously
417 described methods (Kaga et al., 2020; Jhu et al., 2021). *C. campestris* was cultivated on beets
418 in a greenhouse. Shoot tips, approximately 6-8 cm in length, were cut and placed on a 3%
419 agarose plate. Unstimulated shoot tips were flash-frozen at this point for later RNA extraction.
420 Shoot tips "with host" included fresh cut rosette leaves from wild-type (Col-0) *A. thaliana* plants
421 pressed on the tips. Shoot tips were stimulated to form haustoria by weighting with ~8 glass
422 cover slips, exposure to a far-red LED bulb for two hours, followed by four days in complete
423 darkness. The resulting haustoria were collected, flash-frozen, and used for RNA extraction.
424 Total RNA was extracted using a bead-beater and Tri-Reagent (Sigma) per the manufacturer's
425 instructions. Three samples per condition, each from a different plate, were collected and
426 extracted.
427
428 **Small RNA sequencing and analysis**
429 All small RNA-seq libraries were constructed using 500ng of total RNA using the splint-ligation
430 method described by (Maguire et al., 2020). Libraries were sequenced on an Illumina NextSeq

550 (time-course experiments) or NextSeq 2000 (*in vitro* haustoria experiments). Time-course experiment: After de-multiplexing, FASTQ files were trimmed using cutadapt (Martin, 2011) with settings -a AGATCGGAAGAGCACACGTCTGAAC -m 15 --discard-untrimmed. Two concatenated genomes were prepared: *A. thaliana* TAIR10 and *C. campestris* v0.32, and *S. lycopersicum* release 5 and *C. campestris* v0.32. Trimmed reads were aligned to the appropriate concatenated genome using ShortStack (Johnson et al., 2016) version 3.8.5 with setting --align_only. The resulting BAM-formatted alignments were split based on reference genome, to create two BAM files per time-course: One for *C. campestris*, the other for the host genome. These are the alignments hosted at https://plantsmallrnagenes.science.psu.edu/Studies/Hudzik. The *C. campestris* alignments were analyzed using ShortStack version 3.8.5 with a 'locifile' containing the coordinates of all 156 interface-induced *MIRNA* loci (Supplemental Dataset 1). The host-genome alignments were similarly analyzed with a 'locifile' containing locations of known secondary siRNA loci triggered by interface-induced miRNAs (Supplemental Table 3). The resulting count matrices, showing alignments by sample, were combined and processed to yield normalized values in units of read per million mapped. Analysis of small RNA-seq from *in vitro* haustoria was identical except that alignments used only the *C. campestris* genome and no secondary siRNA loci were analyzed.

Analysis of flanking DNA

Upstream and downstream DNA sequences (200 base-pairs each) flanking the 156 interface-induced *MIRNA* loci were retrieved from the version 0.32 *C. campestris* genome assembly (Vogel et al., 2018). Upstream regions were defined to end at the 5' basal DCL cut site; downstream regions were defined to begin at the 3' basal DCL cut site (Figure 4A). Upstream sequences were analyzed with MEME suite (version 5.4.1) (Bailey et al., 2009). Motif discovery with meme used settings '-dna -mod zoops -nmotifs 1 -w 10 -objfun classic -revcomp -markov_order 0'. The top-scoring motif was then used as a query of the upstream sequences with the MEME suite tool fimo using settings '--qv-thresh --thresh 0.05'; this captured all occurrences of the motif with a false-discovery rate of <= 0.05. In a few cases where the motif was found more than once on the same upstream sequence, only the top-scoring instance was retained. The motif consensus sequence is TCCCACA[CT]CG (Figure 4B). The fimo analysis was also run using the upstream regions of conserved, canonical *MIRNA* loci from *C. campestris*; no motif instances were found with an FDR <= 0.05. Motif locations were converted to gff3 format, and then converted to modified gff file with metaplot coordinates based on distance from the 5' basal DCL sites. The subcommand 'genomecov' from the bedtools suite (Quinlan and Hall, 2010) was then used with option -d to calculate position-specific depths. These values were then normalized by dividing by the number of loci in each set (interface-induced *MIRNA* loci or conserved canonical *MIRNA* loci). Moving averages with a window size of 10 were then plotted (Figure 4D). Downstream regions were searched for stretches of six or more T nucleotides on the *MIRNA* coding strand; locations were converted to gff3 format and processed as described above to create metaplots (Figure 4H).

NanoPARE analysis and transcriptional start site inference

Previously described nanoPARE data (Johnson et al., 2019) from *C. campestris* haustorial interfaces with *A. thaliana* stems were retrieved in FASTQ format from the Sequence Read Archive (SRA): Accessions SRR9216111, SRR9216113, and SRR9216114. Contaminating adapter sequences were removed using cutadapt (Martin, 2011) with settings -a CCGAGCCCACGAGACTAAGGCGAATCTCGTATGCCGTCTTCTGCTTG -a CCGAGCCCACGAGACCGTACTAGATCTCGTATGCCGTCTTCTGCTTG -a CCGAGCCCACGAGACAGGCAGAAATCTCGTATGCCGTCTTCTGCTTG -a CCGAGCCCACGAGACGGACTCCTATCTCGTATGCCGTCTTCTGCTTG -a CCGAGCCCACGAGACTAGGCATGATCTCGTATGCCGTCTTCTGCTTG --trim-n -m 20.

482 Trimmed reads were aligned to the version 0.32 *C. campestris* genome assembly (Vogel et al.,
483 2018) using STAR (Dobin et al., 2013) with settings --outFilterMismatchNmax 999 --
484 outFilterMismatchNoverReadLmax 0.07 --outWigType wiggle read1_5p --outWigNorm None.
485 The two resulting .wiggle formatted files contained the depths of RNA 5' ends genome-wide;
486 these files were converted to bigwig format using wigToBigWig (Kent et al., 2010). The bigwig
487 files were then queried to retrieve data from the 200 base-pair upstream regions of each of the
488 interface-induced *MIRNA* loci and each of the conserved canonical *MIRNA* loci using
489 bigWigToBedGraph (Kent et al., 2010). The read depths for each locus were scaled by reads /
490 total reads; this scaled the data so that each locus had equal weight. Actual coordinates were
491 converted to metaplot coordinates based on distance from 5' basal DCL sites. Scaled depths
492 were normalized by dividing by the number of loci in each set (interface-induced *MIRNA* loci or
493 conserved canonical *MIRNA* loci). Moving averages with a window size of 10 were then plotted
494 (Figure 4E). Transcriptional start sites of interface-induced *MIRNA* primary transcripts were
495 inferred to be the maximum nanoPARE read depth location in the 200 base-pair upstream
496 regions; ties were broken randomly.
497
498 **Agroinfiltration of interface-induced *MIRNA* loci**
499 Synthetic double-stranded DNA fragments based on the genomic sequences of two *C.*
500 *campestris* interface-induced *MIRNA* loci were synthesized: ccm-*MIR12463a* and ccm-
501 *MIR12497f*. Two versions of each were constructed: wild-type, and a version where the ten
502 base-pair USE was randomly scrambled. Synthetic DNA fragments were golden-gate cloned
503 into vector pGGZ001 (Lampropoulos et al., 2013) using sites 'A' and 'G'. The T-DNA regions
504 were confirmed by Sanger sequencing. Complete plasmid sequences are in Supplemental
505 Dataset 5. Plasmids were transformed into *Agrobacterium tumefacians* GV3101-pMP90-pSoup.
506 Agroinfiltration into *Nicotiana benthamiana* leaves was performed as previously described (Liu
507 et al., 2014). Leaf samples from infiltrated areas were collected four days after infiltration and
508 processed for total RNA extraction. Total RNA was extracted using one of the following
509 methods: Tri-Reagent (Sigma), New England Biolabs Monarch Total RNA Miniprep Kit (T2010),
510 or Zymo Quick-RNA Plant Miniprep kit (R2024). RNA samples were diluted to 100ng/ul, and
511 used in stem-loop reverse-transcription reactions (Yang et al., 2014) using primers specific to
512 the target miRNA, and to miR159 (which served as a reference gene). Stem-loop reverse
513 transcription primers were self-annealed at 100uM concentration in IDT Duplex Buffer (100mM
514 potassium acetate, 30mM HEPES pH7.5) by heating in a 94C heat block for two minutes
515 followed by de-activation of the heat block for slow cooling to room temperature. Self-annealed
516 primers were diluted to 50nM stocks in water and stored at –20C. Reverse transcription
517 reactions contained 4ul total RNA (at 100ng/ul), 2ul of a freshly prepared stem-loop primer
518 mixture that had each primer at 5nM concentration, 2ul of 5X reverse transcriptase buffer, 1ul of
519 100mM DTT, 0.5ul of 10mM dNTP, and 0.5ul of Protoscript II reverse transcriptase (New
520 England Biolabs M0368). Reverse transcription reactions were incubated at 16C for 20 minutes,
521 42C for 60 minutes, and 80C for five minutes. 1.5ul of the resulting cDNA was used as template
522 in 20ul scale qPCR reactions using Luna Universal qPCR master mix (New England Biolabs
523 M3003) with forward primers specific to the microRNA of interest and a universal reverse
524 primer. PCR conditions for miR12463 detection were 95C for 60 seconds (initial denaturation),
525 95C 5 seconds (denature), 55C 15 seconds (anneal), 70C 10 seconds (extend and detect).
526 PCR conditions for miR12497 detection were 95C for 60 seconds (initial denaturation), 95C 15
527 seconds (denature), 52C 15 seconds (anneal), 72C 30 seconds (extend and detect). Reaction
528 efficiencies for each miRNA were calculated by serial dilution of positive cDNA samples.
529 Efficiency-corrected accumulation relative to miR159 was calculated using the method of (Pfaffl,
530 2001). Primer sequences are in Supplemental Table 4.
531
532 **Accession Numbers**

Newly created small RNA-seq data have been deposited at NCBI GEO under accessions GSE184641, GSE184642, and GSE205256. Accession numbers for each specific library analyzed are in Supplemental Table 1.

Supplemental Data Files

Supplemental Figure 1. *C. campestris* growth on *A. thaliana* stems.

Supplemental Figure 2. *C. campestris* growth on *S. lycopersicum* hypocotyls.

Supplemental Table 1. Small RNA-seq datasets used in this study.

Supplemental Table 2. *trans*-species microRNA families in *Cuscuta campestris*

Supplemental Table 3. Secondary siRNA loci in tomato and *A. thaliana*.

Supplemental Table 4. Oligonucleotide sequences

Supplemental Dataset 1. Annotations of *Cuscuta campestris* interface-induced *MIRNA* loci. Includes mature microRNAs and stem-loop precursors. Reference genome is assembly version 0.32 from (Vogel et al., 2018), retrieved from https://plabipd.de/project_cuscuta2/start.ep Format: general feature format version 3 (gff3).

Supplemental Dataset 2. *C. campestris* interface-induced *MIRNA* hairpin sequences. Format: FASTA.

Supplemental Dataset 3. *C. campestris* interface-induced mature miRNA sequences. Both the 5p and 3p miRNAs are included for each locus. These are the actually sequenced miRNA sequences; in a few cases there are polymorphisms between the actual sequences and the corresponding sequence in the reference genome. This likely reflects polymorphisms between the strain of *C. campestris* used in this study relative to the reference genome specimen. Format: FASTA.

Supplemental Dataset 4. Annotations of *Cuscuta campestris* conserved canonical *MIRNA* loci. Includes mature microRNAs and stem-loop precursors. Reference genome is assembly version 0.32 from (Vogel et al., 2018), retrieved from https://plabipd.de/project_cuscuta2/start.ep Format: general feature format version 3 (gff3).

Supplemental Dataset 5. Sequences and annotations of interface-induced *MIRNA* vectors used in agroinfiltration. Genbank flatfile format (text).

Acknowledgements

We thank the Huck Institutes Genomics Core Facility for small RNA-seq support and Shawn Burghard for Greenhouse services. This research was supported by awards to MJA from the US National Science Foundation (Award # 2003315) and from the US Department of Agriculture – National Institute of Food and Agriculture (Award # 2018-67013-285).

Author Contributions

MJA and CH conceived the project and planned the experiments. MJA and CH conducted most experiments, analyzed data, crafted figures, and wrote the manuscript. SM and SG performed small RNA sequencing. JH made the initial discovery of the upstream sequence element.

584
585 **Conflict of Interest**
586 SM and SG are employees of New England Biolabs, Inc. New England Biolabs is a
587 manufacturer and vendor of molecular biology reagents, including several enzymes and buffers
588 used in this study. This affiliation does not affect the authors' impartiality, adherence to journal
589 standards and policies, or availability of data. CH, JH, and MJA declare no conflicts of interest.
590

Supplemental Figure 1. *C. campestris* growth on *A. thaliana* stems. Cross-sections of toludine blue stained vibratome sections for days 0-15 following parasite coiling. Days 2, 3, and 6 were used as Figure 1 A, B, and C, respectively. Scale bars: 200µm.

595

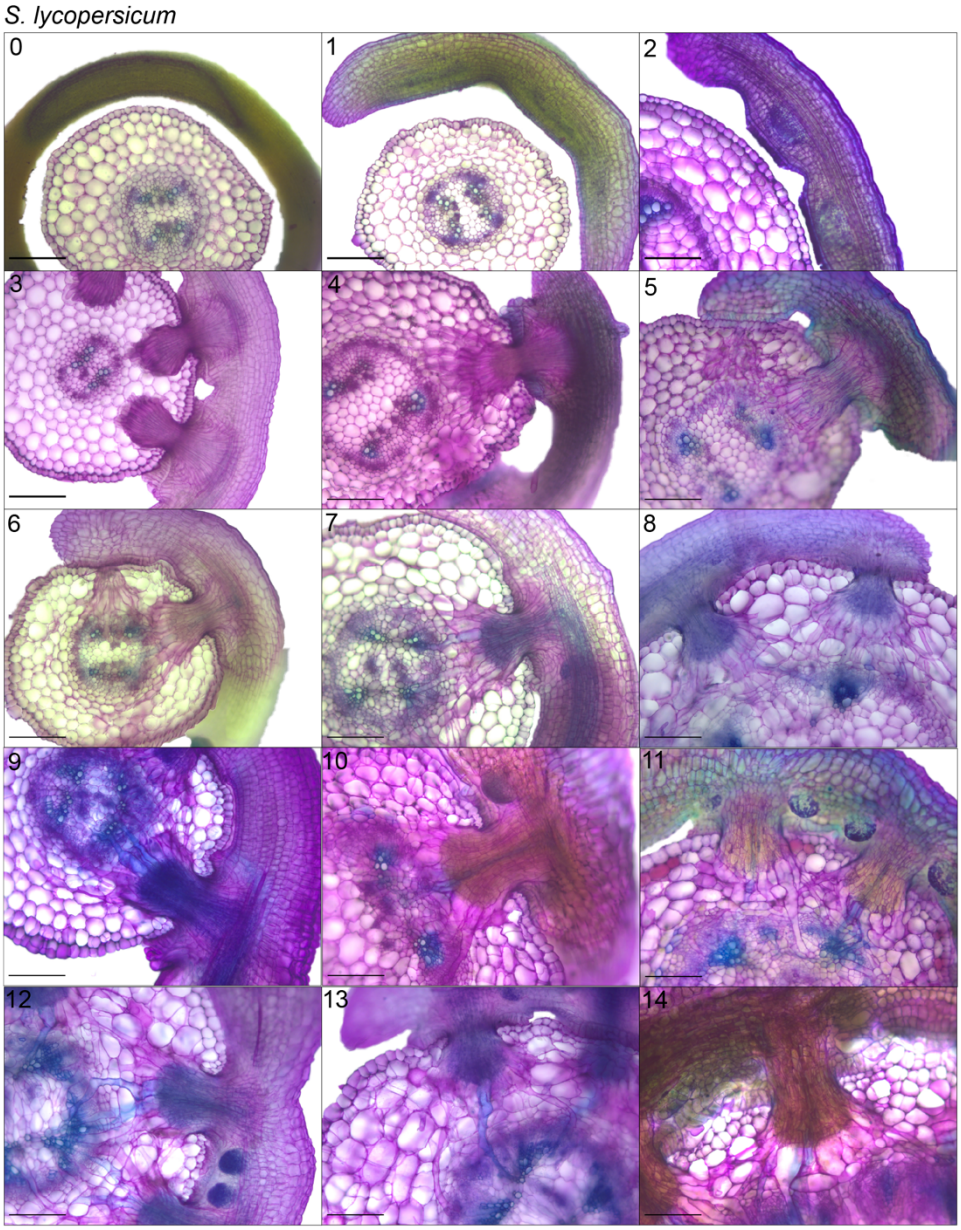

596
597 **Supplemental Figure 2.** *C. campestris* growth on *S. lycopersicum* hypocotyls. Cross-sections

598 of toludine blue stained vibratome sections for days 0-15 following parasite coiling. Days 2, 3,
599 and 6 were used as Figure 1 D, E, and F, respectively Scale bars: 200µm.
600
601
602 **References**

603 **Atkinson JA, Wells DM** (2017) An Updated Protocol for High Throughput Plant Tissue
604 Sectioning. Front Plant Sci **8**: 1721

605 **Axtell MJ** (2013) Classification and comparison of small RNAs from plants. Annual review of
606 plant biology **64**: 137–159

607 **Axtell MJ, Meyers BC** (2018) Revisiting Criteria for Plant MicroRNA Annotation in the Era of
608 Big Data. The Plant cell **30**: 272–284

609 **Bailey TL, Boden M, Buske FA, Frith M, Grant CE, Clementi L, Ren J, Li WW, Noble WS**
610 (2009) MEME SUITE: tools for motif discovery and searching. Nucleic Acids Res **37**:
611 W202-208

612 **Birschwilks M, Haupt S, Hofius D, Neumann S** (2006) Transfer of phloem-mobile substances
613 from the host plants to the holoparasite Cuscuta sp. Journal of Experimental Botany **57**:
614 911–921

615 **Cai Q, Qiao L, Wang M, He B, Lin F-M, Palmquist J, Huang S-D, Jin H** (2018) Plants send
616 small RNAs in extracellular vesicles to fungal pathogen to silence virulence genes.
617 Science **360**: 1126–1129

618 **Chen H-M, Chen L-T, Patel K, Li Y-H, Baulcombe DC, Wu S-H** (2010) 22-Nucleotide RNAs
619 trigger secondary siRNA biogenesis in plants. Proceedings of the National Academy of
620 Sciences of the United States of America **107**: 15269–15274

621 **Chen X** (2005) MicroRNA biogenesis and function in plants. FEBS Lett **579**: 5923–5931

622 **Cuperus JT, Carbonell A, Fahlgren N, Garcia-Ruiz H, Burke RT, Takeda A, Sullivan CM,**
623 **Gilbert SD, Montgomery TA, Carrington JC** (2010) Unique functionality of 22-nt
624 miRNAs in triggering RDR6-dependent siRNA biogenesis from target transcripts in
625 Arabidopsis. Nature structural & molecular biology **17**: 997–1003

626 **David-Schwartz R, Runo S, Townsley B, Machuka J, Sinha N** (2008) Long-distance transport
627 of mRNA via parenchyma cells and phloem across the host–parasite junction in
628 Cuscuta. The New phytologist **179**: 1133–1141

629 **Dobin A, Davis CA, Schlesinger F, Drenkow J, Zaleski C, Jha S, Batut P, Chaisson M,**
630 **Gingeras TR** (2013) STAR: ultrafast universal RNA-seq aligner. Bioinformatics **29**: 15–
631 21

632 **Fei Q, Xia R, Meyers BC** (2013) Phased, secondary, small interfering RNAs in
633 posttranscriptional regulatory networks. The Plant cell **25**: 2400–2415

634 **Gao Z, Herrera-Carrillo E, Berkhout B** (2018) Delineation of the Exact Transcription
635 Termination Signal for Type 3 Polymerase III. Molecular Therapy - Nucleic Acids **10**: 36–
636 44

637 **Heide-Jørgensen H** (2008) Parasitic flowering plants. doi: 10.1163/ej.9789004167506.i-438

638 **Hou Y, Zhai Y, Feng L, Karimi HZ, Rutter BD, Zeng L, Choi DS, Zhang B, Gu W, Chen X,**
639 **Ye W, Innes RW, Zhai J, Ma W** (2019) A Phytophthora Effector Suppresses Trans-
640 Kingdom RNAi to Promote Disease Susceptibility. Cell Host & Microbe **25**: 153-165.e5

641 **Huang C-Y, Wang H, Hu P, Hamby R, Jin H** (2019) Small RNAs - Big Players in Plant-Microbe
642 Interactions. Cell Host Microbe **26**: 173–182

643 **Hudzik C, Hou Y, Ma W, Axtell MJ** (2020) Exchange of small regulatory RNAs between plants
644 and their pests. Plant Physiol **182**: 51–62

645 **Jhu M-Y, Ichihashi Y, Farhi M, Wong C, Sinha NR** (2021) *LATERAL ORGAN BOUNDARIES*
646 *DOMAIN 25* functions as a key regulator of haustorium development in dodders. Plant
647 Physiology **186**: 2093–2110

648 **Johnson NR, dePamphilis CW, Axtell MJ** (2019) Compensatory sequence variation between
649 trans-species small RNAs and their target sites. eLife **8**: e49750

650 **Johnson NR, Yeoh JM, Coruh C, Axtell MJ** (2016) Improved placement of multi-mapping
651 small RNAs. G3 (Bethesda, Md) **6**: 2103–2111

652 **Kaga Y, Yokoyama R, Sano R, Ohtani M, Demura T, Kuroha T, Shinohara N, Nishitani K**
653 (2020) Interspecific Signaling Between the Parasitic Plant and the Host Plants Regulate
654 Xylem Vessel Cell Differentiation in Haustoria of Cuscuta campestris. Front Plant Sci **11**:
655 193

656 **Kent WJ, Zweig AS, Barber G, Hinrichs AS, Karolchik D** (2010) BigWig and BigBed:
657 enabling browsing of large distributed datasets. Bioinformatics **26**: 2204–2207

658 **Kim G, Westwood JH** (2015) Macromolecule exchange in Cuscuta-host plant interactions.
659 Current opinion in plant biology **26**: 20–25

660 **Lampropoulos A, Sutikovic Z, Wenzl C, Maegele I, Lohmann JU, Forner J** (2013)
661 GreenGate---a novel, versatile, and efficient cloning system for plant transgenesis. PLoS
662 ONE **8**: e83043

663 **Langmead B, Trapnell C, Pop M, Salzberg SL** (2009) Ultrafast and memory-efficient
664 alignment of short DNA sequences to the human genome. Genome biology **10**: R25

665 **Liu Q, Wang F, Axtell MJ** (2014) Analysis of complementarity requirements for plant microRNA
666 targeting using a Nicotiana benthamiana quantitative transient assay. The Plant cell **26**:
667 741–753

668 **Love MI, Huber W, Anders S** (2014) Moderated estimation of fold change and dispersion for
669 RNA-seq data with DESeq2. Genome biology **15**: 550

670 **Lowder LG, Malzahn A, Qi Y** (2018) Plant Gene Regulation Using Multiplex CRISPR-dCas9
671 Artificial Transcription Factors. Methods in molecular biology (Clifton, NJ) **1676**: 197–214

672 **Maguire S, Lohman GJS, Guan S** (2020) A low-bias and sensitive small RNA library
673 preparation method using randomized splint ligation. Nucleic Acids Research gkaa480

674 **Martin M** (2011) Cutadapt removes adapter sequences from high-throughput sequencing reads.
675 EMBnet. journal

676 **Matzke MA, Mosher RA** (2014) RNA-directed DNA methylation: an epigenetic pathway of
677 increasing complexity. Nature reviews Genetics **15**: 394–408

678 **Pfaffl MW** (2001) A new mathematical model for relative quantification in real-time RT-PCR.
679 Nucleic acids research **29**: e45

680 **Quinlan AR, Hall IM** (2010) BEDTools: A flexible suite of utilities for comparing genomic
681 features. Bioinformatics **26**: 841–2

682 **Robinson JT, Thorvaldsdóttir H, Winckler W, Guttman M, Lander ES, Getz G, Mesirov JP**
683 (2011) Integrative genomics viewer. Nat Biotechnol **29**: 24–26

684 **Roney JK, Khatibi PA, Westwood JH** (2007) Cross-species translocation of mRNA from host
685 plants into the parasitic plant dodder. Plant physiology **143**: 1037–1043

686 **Shahid S, Kim G, Johnson NR, Wafula E, Wang F, Coruh C, Bernal-Galeano V, Phifer T,**
687 **dePamphilis CW, Westwood JH, Axtell MJ** (2018) MicroRNAs from the parasitic plant
688 Cuscuta campestris target host messenger RNAs. Nature **553**: 82–85

689 **Shimizu K, Aoki K** (2019) Development of Parasitic Organs of a Stem Holoparasitic Plant in
690 Genus Cuscuta. Front Plant Sci **10**: 1435

691 **Subhankar B, Yamaguchi K, Shigenobu S, Aoki K** (2021) *Trans*-species small RNAs move
692 long distances in a parasitic plant complex. Plant Biotechnology **38**: 187–196

693 **Sun G, Xu Y, Liu H, Sun T, Zhang J, Hettenhausen C, Shen G, Qi J, Qin Y, Li J, Wang L,**
694 **Chang W, Guo Z, Baldwin IT, Wu J** (2018) Large-scale gene losses underlie the
695 genome evolution of parasitic plant Cuscuta australis. Nature communications **9**: 2683

696 **Tsutsui H, Higashiyama T** (2017) pKAMA-ITACHI Vectors for Highly Efficient CRISPR/Cas9-
697 Mediated Gene Knockout in Arabidopsis thaliana. Plant Cell Physiol **58**: 46–56

698 **Vankan P, Filipowicz W** (1989) A U-snRNA gene-specific upstream element and a -30 'TATA
699 box' are required for transcription of the U2 snRNA gene of Arabidopsis thaliana. The
700 EMBO Journal **8**: 3875–3882

701 **Vaughn KC** (2003) Dodder hyphae invade the host: a structural and immunocytochemical
702 characterization. Protoplasma **220**: 189–200

703 **Vaughn KC** (2006) Conversion of the Searching Hyphae of Dodder into Xylic and Phloic
704 Hyphae: A Cytochemical and Immunocytochemical Investigation. International Journal of
705 Plant Sciences **167**: 1099–1114

706 **Vogel A, Schwacke R, Denton AK, Usadel B, Hollmann J, Fischer K, Bolger A, Schmidt**
707 **MH-W, Bolger ME, Gundlach H, Mayer KFX, Weiss-Schneeweiss H, Temsch EM,**

708 **Krause K** (2018) Footprints of parasitism in the genome of the parasitic flowering plant
709 Cuscuta campestris. Nature communications **9**: 2515

710 **Waibel F, Filipowicz W** (1990a) U6 snRNA genes of Arabidopsis are transcribed by RNA
711 polymerase III but contain the same two upstream promoter elements as RNA
712 polymerase II-transcribed U-snRNA genes. Nucleic acids research **18**: 3451–3458

713 **Waibel F, Filipowicz W** (1990b) RNA-polymerase specificity of transcription of Arabidopsis U
714 snRNA genes determined by promoter element spacing. Nature **346**: 199

715 **Weiberg A, Wang M, Lin F-M, Zhao H, Zhang Z, Kaloshian I, Huang H-D, Jin H** (2013)
716 Fungal small RNAs suppress plant immunity by hijacking host RNA interference
717 pathways. Science (New York, NY) **342**: 118–123

718 **Xie Z, Allen E, Fahlgren N, Calamar A, Givan SA, Carrington JC** (2005) Expression of
719 Arabidopsis MIRNA genes. Plant physiology **138**: 2145–2154

720 **Yang L, Wang S, Tang L, Liu B, Ye W, Wang L, Wang Z, Zhou M, Chen B** (2014) Universal
721 stem-loop primer method for screening and quantification of microRNA. PloS one **9**:
722 e115293

723 **Yang Z, Wafula EK, Kim G, Shahid S, McNeal JR, Ralph PE, Timilsena PR, Yu W, Kelly EA,**
724 **Zhang H, Person TN, Altman NS, Axtell MJ, Westwood JH, dePamphilis CW** (2019)
725 Convergent horizontal gene transfer and cross-talk of mobile nucleic acids in parasitic
726 plants. Nature Plants **5**: 991–1001

727 **Zangishei Z, Annacondia ML, Gundlach H, Didriksen A, Bruckmüller J, Salari H, Krause**
728 **K, Martinez G** (2022) Parasitic plant small RNA analyses unveil parasite-specific
729 signatures of microRNA retention, loss, and gain. Plant Physiology kiac331

730 **Zhang T, Zhao Y-L, Zhao J-H, Wang S, Jin Y, Chen Z-Q, Fang Y-Y, Hua C-L, Ding S-W,**
731 **Guo H-S** (2016) Cotton plants export microRNAs to inhibit virulence gene expression in
732 a fungal pathogen. Nature Plants **2**: 16153

733